Journal of
Applied Remote Sensing

RemoteSensing.SPIEDigitalLibrary.org

Synergistic retrieval model of forest biomass using the integration of optical and microwave remote sensing

Linjing Zhang
Zhenfeng Shao
Chunyuan Diao

SPIE.

Synergistic retrieval model of forest biomass using the integration of optical and microwave remote sensing

Linjing Zhang,[a,b] Zhenfeng Shao,[a,b,*] and Chunyuan Diao[c]

[a]Wuhan University, State key Laboratory for Information Engineering in Surveying, Mapping and Remote Sensing, 129 Luoyu Road, Wuhan 430079, China

[b]Collaborative Innovation Center for Geospatial Technology, 129 Luoyu Road, Wuhan 430079, China

[c]The State University of New York, University at Buffalo, Department of Geography, 105 Wilkeson Quad, Buffalo, New York 14261, United States

Abstract. Accurate estimation of forest aboveground biomass is crucial for monitoring ecosystem responses to environmental change. Passive optical and active microwave remote sensing plays an important role in retrieving the forest biomass. However, optical spectral reflectance gets saturated in the relatively high-density vegetation area and microwave backscattering is largely influenced by the soil underneath when the vegetation coverage is relatively low. Both of these conditions affect the biomass retrieval accuracy. A synergistic biomass retrieval model through the integration of optical (PROSAIL) and microwave (MIMICS) radiative transfer models was put forward. The proposed model unified the vegetation and soil conditions of PROSAIL and MIMICS models, and determined the optical-alone model, microwave-alone model, and the contributions of key optical and microwave factors to biomass retrieval with the simulated database. The database consisted of the optical bidirectional reflectance and full polarization microwave backscattering of the broad-leaved forest canopy under various conditions. The synergistic model was verified by comparing with the ground measurements and the results of the optical-alone and microwave-alone models. The results indicated that the proposed synergistic retrieval model was more effective than the optical-alone or microwave-alone model, and showed considerable potential in forest aboveground biomass retrieval by integrating passive optical and active microwave remote sensing. [DOI: 10.1117/1.JRS.9.096069]

Keywords: synergistic radiative transfer model; biomass; sensitivity analysis; synergistic retrieval algorithm.

Paper 14734 received Dec. 2, 2014; accepted for publication Mar. 4, 2015; published online Mar. 26, 2015.

1 Introduction

Forest aboveground biomass is an important indicator of a forest ecosystem's ability to fix carbon and sequestrate carbon dioxide from the atmosphere.[1] In the International Geosphere-Biosphere Programme, the carbon cycle is emerging as a research hotspot of global change and terrestrial ecosystems. Therefore, accurate estimation of forest aboveground biomass plays an important role in terrestrial carbon accounting and global climate change modeling studies.[2]

Traditional field methods are time-consuming, costly, difficult to implement in remote areas, and only limited to small areas. Due to the ability to collect information over regional and global scales, remote sensing has been increasingly used in estimating forest biomass.[3–9] Lu et al.[10] found that the fifth band of Landsat5 thematic mapper (TM), linear transformed indices, such as the first component in a principal component analysis, the brightness of the tasseled cap transform (TCB),[11] and albedo were most strongly correlated with forest biomass. Mutanga and Skidmore[12] concluded that a simple ratio vegetation index yielded the highest

*Address all correspondence to: Zhenfeng Shao, E-mail: shaozhenfeng@whu.edu.cn

1931-3195/2015/$25.00 © 2015 SPIE

correlation coefficient with biomass as compared to the narrow band normalized difference vegetation index (NDVI) and transformed vegetation index (TVI). Kazar and Warner[13] assessed the potential of several spectral radiances from Landsat5 TM imagery to estimate biomass, including raw red and near-infrared radiances, TCT indices, and four vegetation indices, namely enhanced vegetation index (EVI), soil adjusted vegetation index (SAVI), TVI, and NDVI. Among the spectral radiances examined, they found that TC and EVI were most strongly correlated with biomass. In addition to the passive optical remote sensing, active microwave remote sensing, with its advantages of cloud penetration, all-time and all-weather coverage, has also been explored in estimating the forest biomass. For example, radar backscattering in P- and L- bands has been found to be highly correlated with major forest parameters, such as tree age, tree height (H), the diameter at breast height (DBH), basal area, and biomass.[14–17] Harrell et al.[18] evaluated four techniques for biomass estimation in pine stands using shuttle imaging radar C- and L-bands multipolarization radar data and found that the L-band horizontal-transmit/horizontal-receive (HH) polarization data were the critical elements in biomass estimation. The integration of the L-band HH polarization data and the C-band horizontal-transmit/vertical-receive (HV) (or HH) polarization data in these techniques significantly the improved biomass estimation performance. Englhart et al.[19] investigated the potential of X- and L-bands synthetic aperture radar (SAR) data to estimate aboveground biomass in intact and degraded tropical forests and concluded that the multitemporal L- and X-bands combined model achieved the best results for large-scale biomass estimations in tropical forests.

Although a number of studies have evaluated remote sensing techniques for quantifying biomass, the ability to accurately retrieve forest biomass with passive optical or active microwave remote sensing is still limited. On one hand, passive optical remote sensing can be greatly obscured by frequent cloud cover, rain, and snow. Moreover, optical spectral reflectance will become saturated in high-density canopy vegetation areas. On the other hand, microwave remote sensing can be heavily influenced by soil moisture and soil roughness when the vegetation coverage is relatively low. Given that microwave remote sensing is much less sensitive to atmospheric moisture than optical sensors, it has the advantage of dense vegetation detection.[20,21] Furthermore, optical remote sensing can effectively preserve the spectral information when the vegetation canopy density is not high. Therefore, it is urgently necessary to develop alternative approaches that can combine passive optical with active microwave remote sensing to improve the estimation accuracy of forest biomass and other vegetation parameters.

The main objective of this research is to develop a synergistic retrieval model through the joint simulation using optical and microwave radiative transfer models. Optical and microwave radiative transfer models can simulate the principles and procedures of the interaction between electromagnetic waves and vegetation. This joint simulation will provide the theoretical foundation and guidance for forest biomass estimation.

Specifically, the joint optical and microwave radiative transfer models were built by first unifying the vegetation and soil conditions in the two models. And then the database of optical bidirectional reflectance and full polarization microwave backscattering of the broad-leaved forest were simulated using these two joint models. Based on the joint simulated database, a synergistic biomass retrieval model integrating optical and microwave remote sensing was developed. Finally, the performance of the synergistic retrieval model was evaluated by comparing with the ground measurements and the optical-alone and microwave-alone models results.

2 Study Area and Data

2.1 *Study Area Description*

The study focused on Genhe area in the west of Greater Hinggan which is the largest primeval forest in the north of China. The specific study area (50°48′ N, 121°34′ E), which is part of Genhe area, has an area of 25×25 km^2 (Fig. 1). It is located in the frigid temperate zone and has continental monsoon climate. The annual mean temperature is −5.5°C and the annual mean precipitation is approximately 464 mm, with 63% of that falling between June and August.

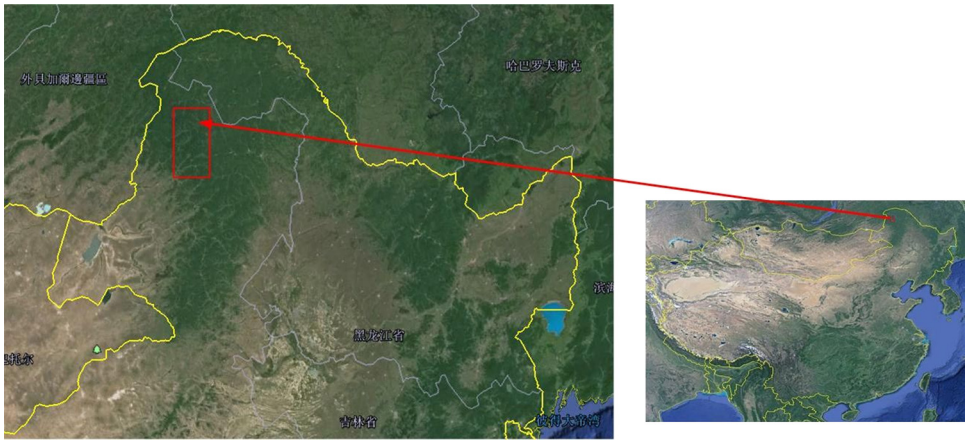

Fig. 1 Geographic location of the study area.

The dominant vegetation type in this area is broad-leaved forest that comprises mostly *Betula*, with some *Larix* spp. and *Pinus sylvestris*.

2.2 *Data Acquisition*

2.2.1 *Remote sensing data*

Two satellite images were used in this experiment: a multispectral image (Landsat5 TM) collected on September 9, 2012, and a RADARSAT-2 image collected on June 30, 2013. RADARSAT-2 is a high-resolution commercial radar satellite that was successfully launched on December 14, 2007, by Canadian Space Agency. The satellite has a SAR with multiple polarization modes, including a fully polarimetric mode in which HH, HV, vertical-transmit/vertical-receive (VV), and vertical-transmit/horizontal-receive (VH) polarized data are acquired. Its frequency is 5.6 GHz (C-band) and the highest resolution is 1 m in spotlight mode (3 m in ultra fine mode) with a 100 m positional accuracy requirement. In this research, a RADARSAT-2 full polarization single-look complex image with a mean incident angle of 36.6 deg was acquired.

2.2.2 *Terrestrial surveying data*

A field survey of the sample plots was conducted from mid-August to early September. In this study, the broad-leaved forest (*Betula*) was taken as the research object without considering the effects of small amounts of coniferous forest. Twelve sample plots (25×25 m^2) were selected and they were all positioned within a homogeneous area far away from the road. Within each plot, for every tree that has a DBH greater than 3 cm, H, leaf area index (LAI), DBH, and crown breadth (CB) were recorded. The tree DBH was measured at 1.3 m above the ground, and the values ranged from 5.0 to 38.2 cm with an average of 13.5 cm. The tree height values varied from 5.1 to 23.8 m with a mean value of 13.35 m.

2.3 *Data Processing*

Remote sensing data and field survey data were processed and the procedures were as follows:

(1) The Landsat5 TM image was radiometrically calibrated to the top of the atmosphere radiance using postlaunch calibration coefficients before then being atmospherically corrected using the atmospheric radiative transfer model: 6S (second simulation of satellite signal in the solar spectrum).[22] The image was then geometrically corrected using the ground control points with an overall error of 0.46 pixels.
(2) The RADARSAT-2 image was radiometrically calibrated to obtain the backscattering coefficients transformed from the digital number using the Next European Space Agency

Table 1 The best-fit allometric model used for estimation of above-ground biomass (AGB).

Regression model	r	p
$W_{stock} = 0.1193(DBH^2H)^{0.8372}$	0.927	<0.05
$W_{branch} = 0.002(DBH^2H)^{1.12}$	0.938	<0.05
$W_{leaf} = 0.000015(DBH^2H)^{1.472}$	0.911	<0.05

Note: W_{stock}, W_{branch}, and W_{leaf} are the biomass of stock, branch, and leaf (kg). DBH and H are the diameters at breast height in centimeters and tree height in meters, respectively.

(ESA) SAR Toolbox (NEST) software.[23] To compensate for speckle noise, the "Enhanced LEE Adaptive Filter" was applied to replace the central pixel of a moving window (3×3 pixels) with the average value for the pixels in the window. The image was then geometrically corrected using the preprocessed TM image with an overall error of 0.56 pixels. The terrain of the site considered in this study was comparatively flat, thus, the terrain correction was not made. After that the RADARSAT-2 image was resampled to the resolution of the TM image (30 m). The TM and RADARSAT-2 images were all resized to match the study area (25×25 km^2).

(3) Based on the tree biophysical data (H, LAI, DBH, and CB) collected from 12 sample plots, the plot biomass was calculated. First, the biomass of each part of each individual tree was calculated by applying the allometric models[24] (Table 1) devised for the broad-leaved forest in the northeast of China based on DBH and H. Second, the biomass of each individual tree was obtained by summing the calculated biomass of its component parts. Third, the biomass of each individual tree in a plot was summed to get the plot biomass. The plot biomass was measured in kilograms (kg). After getting the total biomass of all trees in a plot, the biomass density of a plot was measured in megagrams per hectare (Mg/ha). The total aboveground biomass for each individual plot varied between 76.9 and 159.3 Mg/ha and the mean value for these 12 plots was 100.9 Mg/ha.

3 Methodology

3.1 *Building Simulated Database based on Joint Optical and Microwave Radiative Transfer Models*

3.1.1 *Model introduction*

PROSAIL. The PROSAIL[25] model is a coupled model which includes spectral models for leaf optical properties (PROSPECT) and canopy reflectance (SAIL). PROSPECT is a radiative transfer model based on Allen's generalized "plate model."[26,27] It divides each leaf into N layers, and describes the diffuse radiation in each layer. The reflected radiation of the top layer and the transmitted radiation of the bottom layer are computed by integrating all layers. The advantage of PROSPECT is that the spectral refractive index, determined by the specific absorption of water and pigments,[28] is independent of leaf type. The values are computed by fitting the relation between leaf biochemical parameters and leaf optical spectra.[29] The accuracy of simulated leaf spectra has been extensively validated using the measured spectral data of many kinds of leaf structures.

The SAIL model[30] is based on the Kubelka–Munk theory. This model considers upward and downward solar direct radiation flux and sky diffuse radiation flux. The outgoing radiation flux of the view direction is computed by accounting for the extinction and scattering interactions of canopy constituents. Directional reflectance is described as the ratio of the outgoing radiation flux of the view direction to the total incoming radiation flux. The model assumes that the canopy is continuous and takes into account major factors affecting the radiation flux in plant

canopies, such as LAI, average leaf angle, leaf optical spectra, and soil spectra. Therefore, the simulated canopy reflectance can reflect the real canopy situation to a large degree.

MIMICS. The Michigan Microwave Canopy Scattering (MIMICS) model[31] is based on the first-order solution of the microwave radiation transfer model for a continuous forest canopy. It has been the most widely used theoretical model to study vegetation scattering properties. The model assumes that the forest comprises three layers: crown, trunk, and ground surface. The primary constituents of the crown layer are leaves and branches which obey a random distribution in the azimuthal direction. The trunk layer is described by cylinders with a certain size and random inclination distribution. The ground layer is simplified as a rough surface. There are four kinds of scattering mechanisms: direct scattering from the crown, direct scattering from the ground, single scattering between the crown and the ground, and dihedral reflection between the trunk and the ground. The MIMICS model is able to simulate the copolarization and cross-polarization microwave backscattering of frequencies ranging from 0.5 to 10 GHz and incidence angles between 10 deg and 70 deg.

3.1.2 *Jointing optical and microwave models and simulating database*

PROSAIL and MIMICS models describe canopy structures, physiological and biochemical characteristics of canopy constituents, soil characteristics, and view geometries in different focuses. According to the differences and relations between the two models, the joint optical and microwave radiative transfer models were built by unifying the vegetation and soil conditions of the two models. Then the database of optical bidirectional reflectance and full polarization microwave backscattering of the broad-leaved forest were acquired using joint simulation.

Unifying leaf water content. The PROSPECT model can construct the relation between leaf biochemical components and spectral characteristics and describe the optical properties of plant leaves from 400 to 2500 nm. Scattering in the PROSPECT model is described using a spectral refractive index (n) and a parameter characterizing the leaf mesophyll structure (N). Absorption is modeled using the pigment concentration (C_{ab}), water content (C_{w}), and the corresponding spectral absorption coefficients (K_{a+b} and K_w). It should be noted that leaf water content in the PROSPECT model is the water content per unit leaf area (C_{w}), but in the MIMICS model, it is defined as the ratio of water content to leaf dry weight, and it is denoted as L_{gmc}. The leaf water content of these two models was unified using specific leaf weight (SLW). The equations for the SLW and leaf water content transition relationship can be written as

$$\mathrm{SLW} = \frac{\mathrm{DW}}{\mathrm{A}}, \tag{1}$$

$$C_{\mathrm{w}} = \mathrm{SLW} \times L_{\mathrm{gmc}}, \tag{2}$$

where DW is the leaf dry weight (g) and A is the leaf area (cm^2).

Unifying soil moisture content. In the study area, the most important factor affecting the soil reflectance was soil moisture content. In the PROSAIL model, soil moisture is defined as soil gravimetric moisture content ($\mathrm{S_{gmc}}$), while in the MIMICS model, it is defined as soil volumetric moisture content ($\mathrm{S_{vmc}}$). These two values can be transformed to each other and unified by using soil bulk density. The measured value of the soil bulk density was 1.01 $\mathrm{g/cm^3}$ in the study area with the cutting ring method.

Unifying canopy structure parameters. As an important canopy structure parameter, leaf spatial distribution has an important effect on both canopy optical reflection and microwave

backscattering. The probability distribution of leaf area inclination was unified by using a simple Beta distribution model.[32] Another important canopy structure parameter in these two models was LAI.[33] In the MIMICS model, LAI was refined into canopy thickness (H_{canopy}), diameter of a leaf (D_{leaf}), and volume density of leaves (N_{leaf}). The conversion equation can be written as

$$\text{LAI} = N_{\text{leaf}} \times H_{\text{canopy}} \times \pi \times \left(\frac{D_{\text{leaf}}}{2}\right)^2 \times 10^{-4}. \quad (3)$$

Model input parameters. In addition to the relevant parameters that needed to be unified using the previously mentioned steps, the values of common parameters and unique parameters in the two models needed to be determined. Leaf reflectance, leaf transmittance, and soil reflectance were important parameters of the PROSAIL model. Leaf spectral characteristics were relevant to C_{ab}, C_{w}, dry matter content (C_{m}), and N. Soil spectral reflectance was relevant to S_{gmc} and texture, while the soil texture was not taken into consideration in this paper. The MIMICS model focused on the characteristics affecting microwave backscattering, such as leaf water content and structure of components, as well as soil moisture and texture. These characteristics can be described by parameters L_{gmc}, D_{leaf}, S_{vmc}, soil surface RMS height (S_{rmsh}), and soil surface correlation length (S_{cl}). The MIMICS model took both needles and broad leaves into consideration. Given that only broad-leaved forest was the research object in the study, the MIMICS model was appropriately modified. According to field measurements (H, LAI, DBH, and CB) and the investigation of the study area, the values of input parameters and the corresponding steps in these two models were listed in Tables 2 and 3.

Through setting up common parameters, unique parameters and relevant parameters, the joint optical and microwave radiative transfer models were built. Then the database of optical bidirectional reflectance and full polarization microwave backscattering of the broad-leaved forest were acquired using joint simulation.

Table 2 Input parameters of the PROSAIL model.

Model		Parameter	Abbreviation	Range of variation	Step
PROSAIL	Common parameter	Mean leaf angle (deg)	ALA	25 to 65	5
		Tree height (m)	H	5 to 40	1
		Stand density (trees/ha)	DEN	200 to 2800	200
	Unique parameter	Wavelength (nm)	λ	400 to 2500	5
		View zenith angle (deg)	θ_v	0 to 50	10
		Solar zenith angle (deg)	θ_s	30	0
		Relative azimuth angle (deg)	φ	0	0
		Chlorophyll concentration (μg/cm^2)	C_{ab}	30.5	0
		Dry matter content (g/cm^2)	C_{m}	0.008	0
		Structural parameters of the leaf	N	1.5	0
		Atmospheric visibility (km)	vis	25	0
	Relevant parameter	Leaf water content (g/cm^2)	C_{w}	Transform by Eq. (2)	—
		Soil gravimetric moisture content (%)	S_{gmc}	Transform by soil bulk density	—
		Leaf area index	LAI	Transform by Eq. (3)	—

Table 3 Input parameters of the MIMICS model.

Model		Parameter	Abbreviation	Range of variation	Step
MIMICS	Common parameters	Mean leaf angle (deg)	ALA	25 to 65	5
		Tree height (m)	H	5 to 40	1
		Stand density (trees/ha)	DEN	200 to 2800	200
	Unique parameters	Frequency (GHz)	f	C-band (5.6 GHz), L-band (1.27 GHz)	—
		Polarization	—	VV, HH, VH, HV	—
		Incidence (deg)	θ	10 to 50	10
		Soil surface RMS height (cm)	S_{rmsh}	2	—
		Soil surface correlation length (cm)	S_{cl}	10	—
		Parameters about stock, branch, and leaf		Table 4	
	Relevant parameters	Leaf water content (%)	L_{gmc}	60 to 90	5
		Soil volumetric moisture content (g/cm^3)	S_{vmc}	0.05 to 0.5	0.05
		Leaf diameter (cm)	D_{leaf}	3.5	—
		Canopy thickness (m)	H_{canopy}	0.5 to 35	—
		Volume density of leaves (n/m^3)	N_{leaf}	2 to 1500	—

Note: VH and HV polarization backscattering coefficients simulated by MIMICS were equal, and thus only VH polarization backscattering was used in this study. H_{canopy} and N_{leaf} were calculated by a series of empirical formulae, thus there were not fixed step.

Table 4 Input parameters about stock, branch, and leaf in the MIMICS model.[31]

Structure		Parameter	Abbreviation
Stock		Diameter (m)	D_stock
		Height (m)	H_stock
Branch	Primary branch	Moisture (%)	M_branch1
		Length (m)	L_branch1
		Diameter (m)	D_branch1
		Density (n/m^3)	DE_branch1
	Secondary branch	Moisture (%)	M_branch2
		Length (m)	L_branch2
		Diameter (m)	D_branch2
		Density (n/m^3)	DE_branch2
Leaf		Thickness (cm)	T_leaf
		Density (n/m^3)	DE_leaf

3.2 *Building a Synergistic Retrieval Model of Biomass*

3.2.1 *Synergistic mechanism analysis*

The key of building the synergistic retrieval model was to determine the weights of optical and microwave data under different vegetation conditions. The optical bidirectional reflectance of the vegetation canopy is affected by the space within canopies and the volume density of components to a large extent. When the vegetation coverage is relatively low, optical bidirectional reflectance can more effectively capture the vegetation information than microwave backscattering. The microwave backscattering is largely influenced by the soil underneath in this scenario, thus the synergistic retrieval model primarily depends on the optical data. On the contrary, in the relatively high-density vegetation areas, optical multiple scattering within canopies will be stronger and optical radiation starts to saturate, which leads to almost constant canopy optical reflectance. In this situation, the strong penetrability of microwave backscattering will beneficial for acquiring more complete canopy parameters information. Therefore, the equation of the synergistic retrieval model can be written as

$$\text{Biomass} = (a \times \text{Index} + b) \times f(\alpha) + [1 - (a \times \text{Index} + b)] \times f(\beta), \tag{4}$$

where $f(\alpha)$ and $f(\beta)$ were the optical-alone and microwave-alone retrieval models, respectively;α and β were the optical and microwave sensitive indices, respectively; index was the optical key factor; a and b were the weighting factors acquired using the sensitivity analysis. The details of the parameters used in this equation were introduced in the following sections.

3.2.2 *Optical retrieval model*

Sensitivity analysis between typical vegetation indices and biomass. The canopy optical reflectance under different biomass conditions was simulated using the PROSAIL model, given that all other parameters (e.g., vegetation biochemical parameters and view geometries) were fixed to the mean values. Figure 2 showed the simulated reflectance curves under different biomass conditions. The wavebands obviously influenced by biomass variation in visible and near-infrared regions contained the wavelengths: 470 ± 5, 550 ± 5, 670 ± 5, 780 ± 5, 900 ± 5, 930 ± 5, 1060 ± 5, 1190 ± 5, and 1260 ± 5 nm.

Optical vegetation indices are usually designed based on the significant difference between near-infrared and red reflectance. Considering the wavebands obviously affected by biomass variation (Fig. 2) and the commonly used vegetation indices, several optical vegetation indices

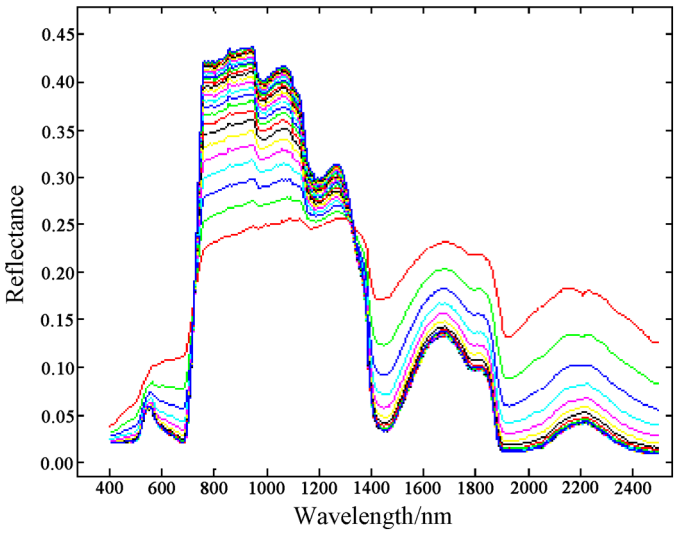

Fig. 2 The canopy reflectance curves under different biomass conditions.

Table 5 Vegetation indices and calculation formulas.

Vegetation index	Formula
MSAVI	$R_{780} + 0.5 - \text{sqrt}[(R_{780} + 0.5) \wedge 2 - 2 \times (R_{780} - R_{670})]$
TVI	$[120 \times (R_{780} - R_{550}) - 200 \times (R_{670} - R_{550})]/2$
NDVI	$((R_{780} - R_{670})/(R_{780} + R_{670})$
RVI	R_{780}/R_{670}
EVI	$2.5 \times (R_{780} - R_{670})/(1 + R_{780} + 6 \times R_{670} - 7.5 \times R_{470})$

were selected, including modified soil adjusted vegetation index (MSAVI), ratio vegetation index (RVI), TVI, NDVI, and EVI (Table 5). Given the influence of soil reflectance, based on the optical simulated database, the impacts of soil moisture content on the relationships between the vegetation indices and biomass were analyzed. Figure 3 showed the correlations between the vegetation indices and biomass under different soil moisture content conditions.

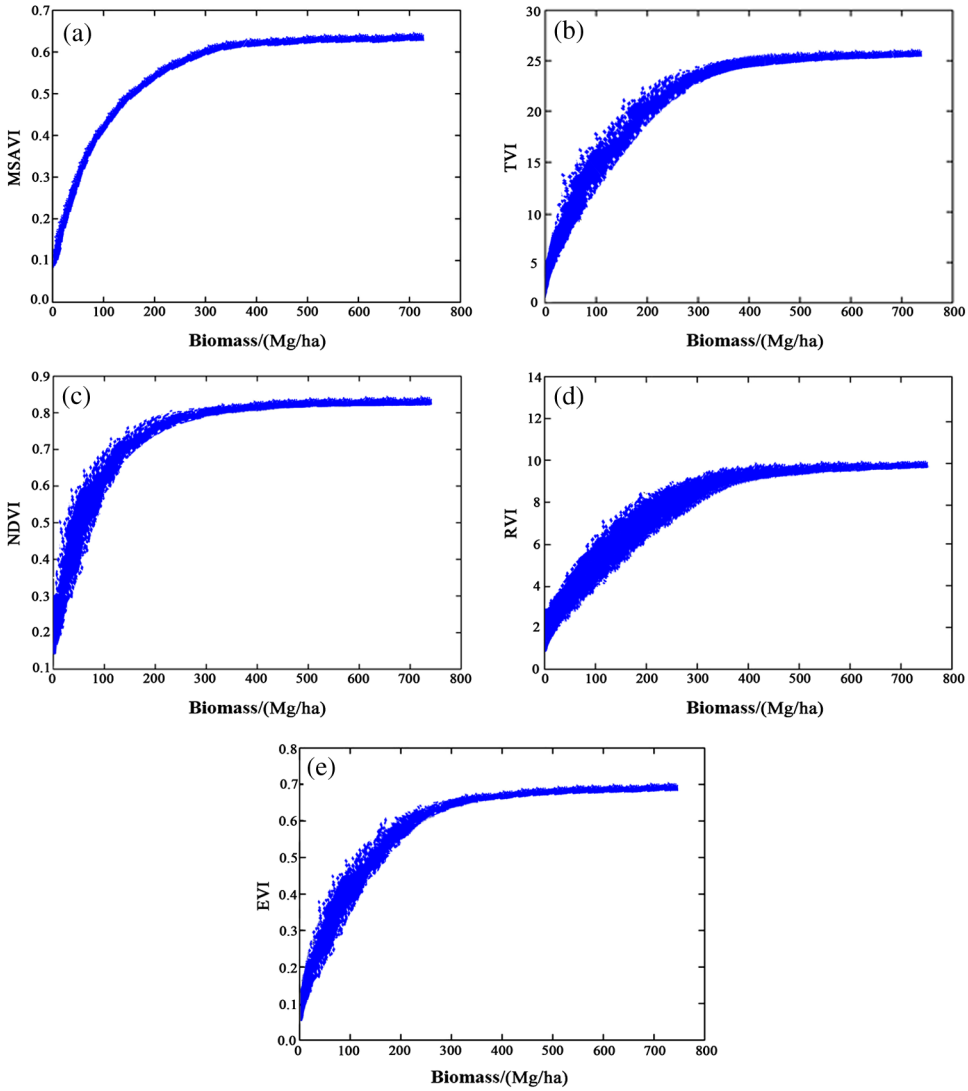

Fig. 3 Sensitivity analysis between biomass and (a) modified soil adjusted vegetation index (MSAVI), (b) transformed vegetation index (TVI), (c) normalized difference vegetation index (NDVI), (d) ratio vegetation index (RVI), (e) enhanced vegetation index (EVI).

Figure 3 illustrated that the values of biomass were between 200 and 300 Mg/ha when the five vegetation indices got saturated. At the saturated location, the value of biomass for NDVI was close to that for EVI. Meanwhile, the values of biomass for MSAVI, TVI, and RVI were similar, but higher than that for the other two indices. Before the vegetation indices got saturated, the rate of change of NDVI was far higher than that of EVI, and the rate of change of MSAVI was higher than that of TVI and RVI. It indicated that NDVI and MSAVI were more sensitive to the change of biomass in this study area. But the impact of soil moisture content on the relationship between NDVI and biomass was conspicuous for the cases of relatively low biomass, while there was little influence on the relationship between MSAVI and biomass. Therefore, MSAVI was chosen as the optimal optical vegetation index for the further regression analysis.

Regression analysis. In Fig. 3, the trend of the scatterplot (a) indicated that the relationship between MSAVI and biomass could be fitted using an exponential model [Eq. (5)]. 96.8% of the variation in biomass could be explained by MSAVI and the root-mean-square error (RMSE), [Eq. (14)], was 23.587. Therefore, MSAVI was taken as the optical sensitive index α, and the regression model between MSAVI and biomass was taken as the optical-alone retrieval model, namely $f(\alpha)$ in Eq. (4).

$$\text{Biomass} = 3.336 \times e^{7.903 \times \text{MSAVI}}. \tag{5}$$

3.2.3 *Microwave retrieval model*

Sensitivity analysis between backscattering and biomass. Using the microwave backscattering coefficients simulated database, the sensitivity was analyzed between the microwave full polarization backscattering coefficients and biomass under different soil moisture content conditions. Different combinations of frequency (C-band or L-band) and polarization (VV, HH, or VH) of the microwave backscattering were explored in the analysis (Fig. 4).

From Fig. 4, the combination of C-band (5.6GHz) and VH polarization, and the combination of L-band (1.27 GHz) and HH (or VH) polarization were found to be more sensitive to the change of biomass. The polarization ratio may enhance the response of microwave backscattering to biomass. Based on these sensitive combinations, three polarization ratios (Ratio1: C-HH/C-VH, Ratio2: L-HH/C-VH, and Ratio3: C-VH/L-VH) were designed in this study. The sensitivity analysis was then conducted between the polarization ratios and biomass (Fig. 5). Figure 5 showed that the sensitivity between the polarization ratio and biomass was the highest in Ratio2, followed by Ratio1, and the lowest in Ratio3. Given the relatively high sensitivity in Ratio1 scenario and the frequency of RADARSAT-2 (only C-band) acquired in the study area, Ratio1 was chosen as the sensitive microwave index and used in the following regression analysis.

Regression analysis. According to the trend of the Ratio1 scatterplot in Fig. 5, the power exponential model was used to fit the relationship between Ratio1 and biomass [Eq. (6)]. 92.6% of the variation in biomass could be explained by Ratio1 and the RMSE was 32.57. Therefore, Ratio1 was taken as the microwave sensitive index β, and the regression model between biomass and Ratio1 was taken as the microwave-alone retrieval model, namely $f(\beta)$ in Eq. (4).

$$\text{Biomass} = 11.512 \times \text{Ratio1}^{(-0.609)}. \tag{6}$$

From Figs. 4 and 5, we can see that the influence of soil moisture content on the relationship between Ratio1 (or the other combinations) and biomass was obvious for the cases of relatively low biomass, and was greatly weakened in the scenario of relatively high biomass. Therefore, considering the relationship between biomass and Ratio1(or MSAVI) and the degree of the impacts of the soil moisture content on Ratio1(or MSAVI), it was significant to determine

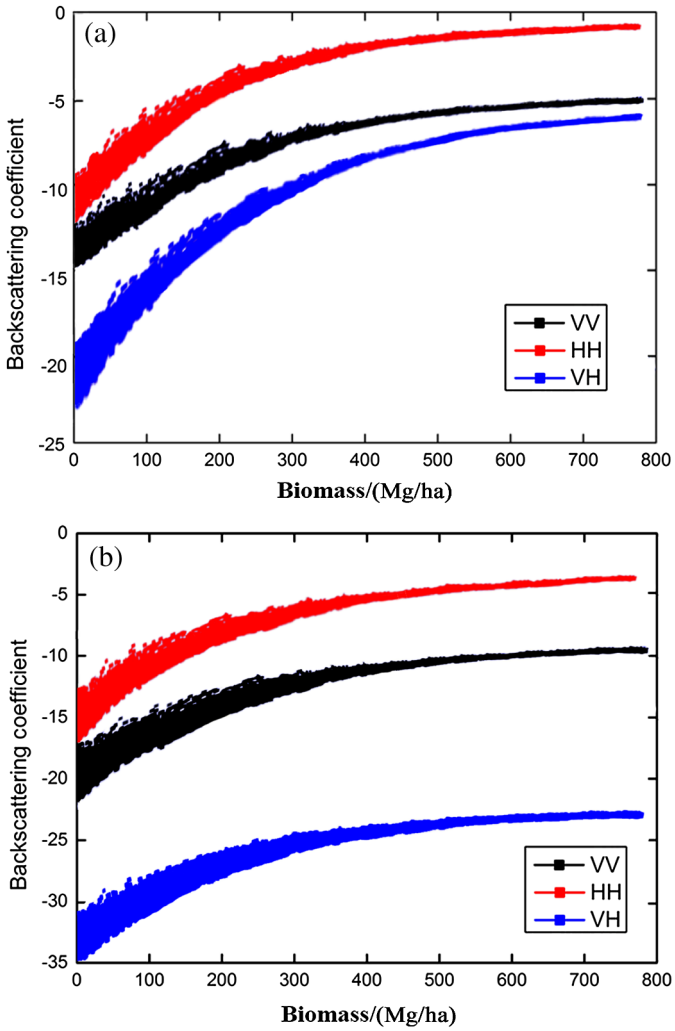

Fig. 4 Sensitivity analysis between biomass and (a) the full polarization backscattering of C-band, (b) the full polarization backscattering of L-band.

the contributions of optical and microwave data in the synergistic retrieval model under different vegetation coverage conditions.

3.2.4 *Calculating the weights of optical and microwave data*

In the synergistic retrieval model, the contributions of optical and microwave data depended on their assigned weights [a and b in Eq. (4)]. Under different vegetation coverage conditions, the sensitivities of optical and microwave data to the variation of biomass were also different. Therefore, in order to estimate the contributions of optical and microwave data under different vegetation densities, the relationship analysis between the sensitivities of optical and microwave key factors (e.g., MSAVI and Ratio1) and biomass was essential. The optical and microwave key factors first needed to be normalized so as to unify their metrics. The normalization processing can be carried out as

$$y_i = \frac{x_i - x_{\min}}{x_{\max} - x_{\min}}, \tag{7}$$

where x_i was the value of the optical (or microwave) key factor under the i'th vegetation condition; $x_{\min}$ and $x_{\max}$ were the minimum and maximum of the optical (or microwave) key factor, respectively; y_i was the corresponding normalized value.

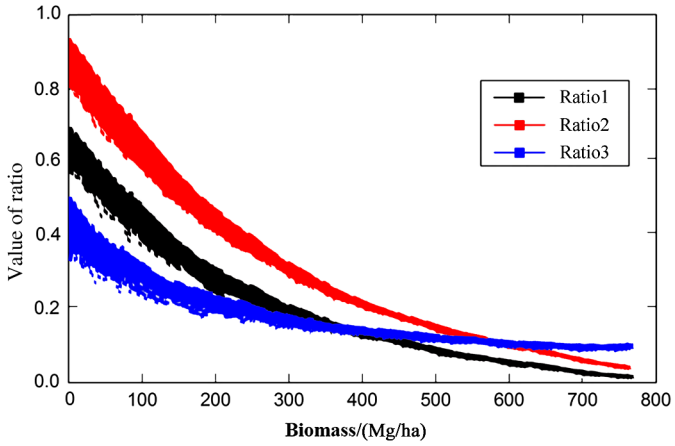

Fig. 5 Sensitivity analysis between biomass and polarization ratios.

Then the sensitivity of the optical (or microwave) key factor can be calculated as follows:

$$\text{Sensitivity} = |y_{i+1} - y_i|, \tag{8}$$

where y_i was the normalized value of the optical (or microwave) key factor under the i'th vegetation condition.

Relationship analysis between MSAVI sensitivity and biomass. According to the previous analysis in Sec. 3.2.2, MSAVI was chosen as the optical key factor, namely Index in Eq. (4). Based on the optical simulated database, the relationship between the sensitivity of MSAVI and the biomass was analyzed (Fig. 6).

Figure 6 showed how the sensitivity of MSAVI changed with the biomass. From Fig. 6, we can see that the sensitivity of MSAVI rose in the first stage, acquired the maximum of 0.15, and then decreased dramatically with the increase of the biomass. The sensitivity of MSAVI was less than 0.02 at the biomass of approximately 200 Mg/ha. When the biomass was more than 400 Mg/ha, MSAVI had lost the ability to respond to the change of biomass. In other words, when the vegetation density increased to a certain level, optical vegetation indices would become saturated.

Relationship analysis between Ratio1 sensitivity and biomass. According to the above analysis in Sec. 3.2.3, the selected microwave key factor in the synergistic retrieval model was Ratio1. Using the simulated microwave backscattering data, the relationship between the sensitivity of Ratio1 and the biomass was analyzed (Fig. 7).

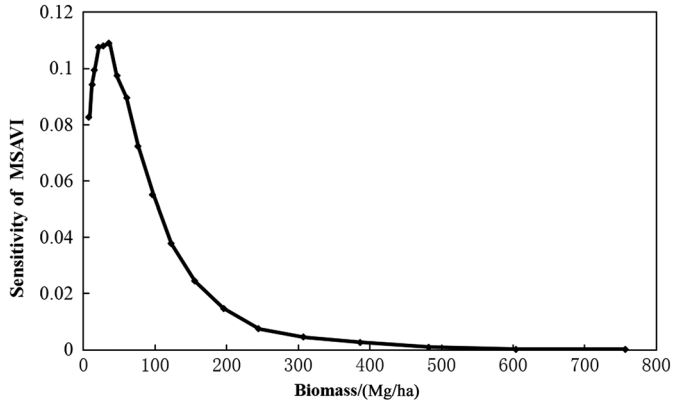

Fig. 6 Relationship between the sensitivity of MSAVI and biomass.

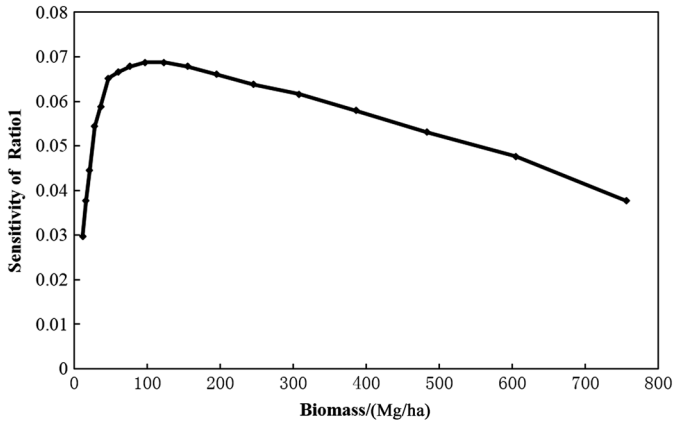

Fig. 7 Relationship between the sensitivity of Ratio1 backscattering and biomass.

Figure 7 illustrated how the sensitivity of Ratio1 changed with the biomass. With the increase of biomass, the sensitivity of Ratio1 first increased, achieved its maximum of 0.07, and then decreased. Compared to the sensitivity of MSAVI (Fig. 6), the overall sensitivity of Ratio1 was much lower.

Based on the analysis above, the optical vegetation index (MSAVI) was found to have a higher sensitivity to biomass than the microwave index (Ratio1), but the saturation of the optical data was also obvious. When the biomass was less than 100 Mg/ha, MSAVI had a higher sensitive to the change of biomass than Ratio1 and played a more important role in the synergistic model. When the value of biomass exceeded 100 Mg/ha, the sensitivity of Ratio1 was higher than that of MSAVI. To determine the weights of optical and microwave data under different vegetation conditions, the ratio of the MSAVI sensitivity to the Ratio1 sensitivity was selected and calculated.

Calculating the weight. Based on the relationship analysis between the sensitivity of optical (or microwave) key factor and biomass, the weights of optical and microwave data can be calculated as

$$OW_i = OS_i/(OS_i + MS_i), \tag{9}$$

$$OW_i + MW_i = 1, \tag{10}$$

where OW_i was the weight of optical data under the i'th biomass condition, and MW_i was the corresponding weight of microwave data; OS_i and MS_i were the sensitivity of MSAVI and the

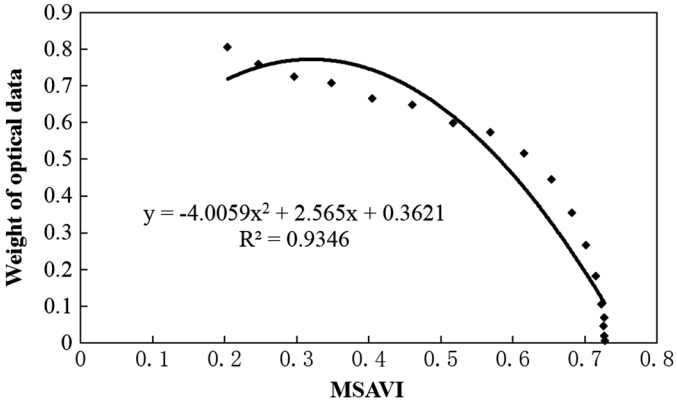

Fig. 8 Statistical relationship between the weight of the optical data and MSAVI.

sensitivity of Ratio1, respectively, and the equation of the sensitivity has been introduced in Eq. (8).

In order to obtain the mathematical expression of the weight of optical data, the relationship between the weight of optical data and corresponding MSAVI under different biomass conditions was acquired using statistic regression analysis (Fig. 8). When MSAVI and Ratio1 were chosen as the key optical and microwave factors, respectively, the weights of the optical and microwave data could be shown as

$$OW(x_i) = (-4.0059) \times x_i^2 + 2.565 \times x_i + 0.3621, \tag{11}$$

$$MW(x_i) = 1 - OW(x_i), \tag{12}$$

where x_i was the value of MSAVI under the i'th biomass condition; $OW(x_i)$ and $MW(x_i)$ were the corresponding weights of optical and microwave data, respectively.

4 Biomass Estimation and Precision Verification

With TM and RADARSAT-2 images, biomass was estimated using the previously developed synergistic retrieval model. The biomass map in the study area was shown in Fig. 9. The dark areas in the figure were rivers areas that have been masked out in the analysis. The maximum forest biomass was 163.82 Mg/ha and was mainly distributed in the northeast of the study area. The minimum forest biomass was 22.36 Mg/ha and was mainly distributed in the northwestern study area. In most of the study area, the biomass was in the range from 65 to 95 Mg/ha.

To investigate the performance of the proposed synergistic retrieval model, the estimated results of biomass from the synergistic model were compared with the field measurements. Furthermore, the estimated results from the synergistic model were also compared with that from the optical-alone retrieval model [Eq. (5)] and the microwave-alone retrieval model [Eq. (6)]. The comparison results were shown in Fig. 10. Table 6 was the comparison results of the error analysis. The retrieval accuracy (M) and RMSE could be calculated as follows:

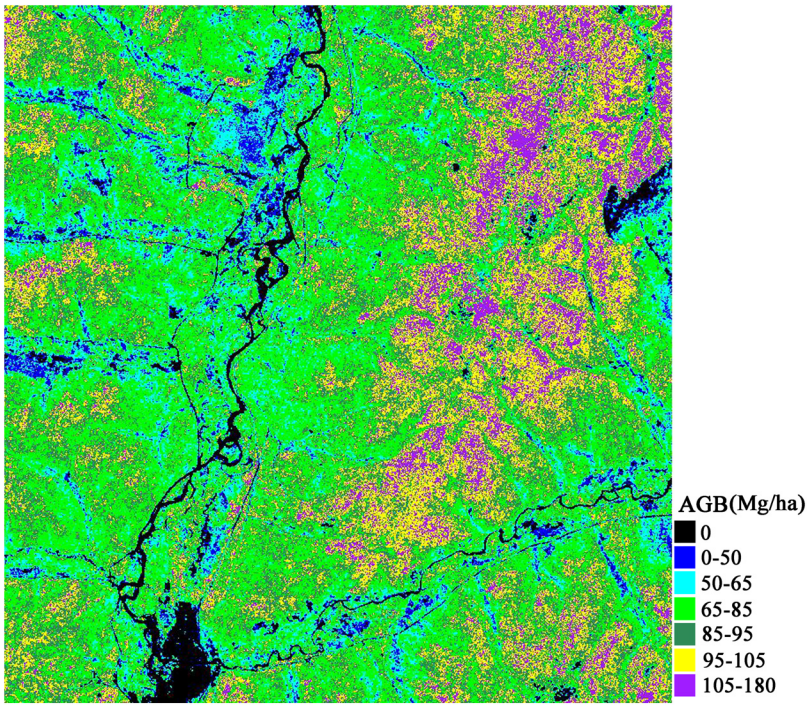

Fig. 9 The retrieval image of biomass with the proposed synergistic model.

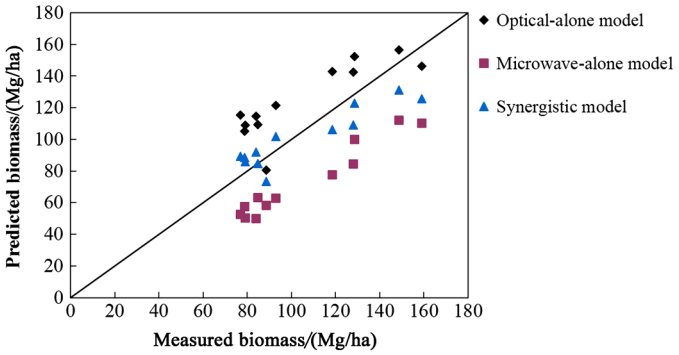

Fig. 10 Comparisons of biomass retrieval results from the synergistic, optical-alone, and microwave-alone models.

Table 6 The estimation precision of the synergistic, the optical-alone and the microwave-alone models.

Model	M (%)	RMSE
Synergy	85.90	14.91
Optical-alone	81.10	19.99
Microwave-alone	70.25	30.58

$$M = \left[1 - \frac{\sum_{i=1}^{n}(|Y_i - X_i|/Y_i)}{n}\right] \times 100\%, \tag{13}$$

$$\mathrm{RMSE} = \sqrt{\frac{1}{n}\sum_{i=1}^{n}(Y_i - X_i)^2}, \tag{14}$$

where X_i and Y_i were the model-predicted biomass and the field biomass on the i'th plot, respectively; n was the number of plots.

The performance of the synergistic retrieval model ($M = 85.90\%$, RMSE $= 14.91$) was found to be obviously better than that of the optical-alone model ($M = 81.10\%$, RMSE $=$ 19.99) or the microwave-alone model ($M = 70.25\%$, RMSE $= 30.58$). These results indicated that the synergistic use of the optical and microwave data could combine their respective advantages in estimating the forest biomass. The complementary effects of the optical and microwave data could contribute to a higher predicted accuracy for forest biomass estimation.

5 Conclusions and Future Work

By unifying the input parameters of the PROSAIL and MIMICS models, joint simulations of optical bidirectional reflectance and microwave backscattering of the same broad-leaved forest canopy and underlying ground surface were performed. Based on the simulated database, a synergistic retrieval model was built to predict the forest biomass in the study area. The field measurements were used to test the validity of this synergistic use of passive optical and active microwave remote sensing. The conclusions were summarized below.

(1) The comparisons between the optical-alone (or microwave-alone) retrieval model and the synergistic retrieval model demonstrated that the model proposed was more effective for forest biomass estimation. The synergistic use of passive optical and active microwave remote sensing showed considerable potential in estimating the forest biomass.

(2) Based on the proposed joint radiative transfer models with the unified input parameters, joint simulations of optical bidirectional reflectance and microwave backscattering provided a basic-ideal database for analyzing the sensitivity of key factors to the change of forest biomass in optical and microwave bands, and developing the corresponding optical and microwave synergistic model.
(3) According to the relationship analysis between the sensitivity of optical (or microwave) key factor and biomass, the weight of optical (or microwave) data in the synergistic retrieval model was determined, which revealed the synergistic mechanism between optical and microwave data.

The effects of curved leaves and multiple scattering within canopies in the MIMICS model were not considered at present, which may reduce the vegetation information provided by microwave data in the synergistic retrieval. Further research work will be focused on how to solve the second-order solution of the microwave radiative transfer model in order to improve the precision of backscattering coefficients simulating.

Acknowledgments

This work was supported by the National Science and Technology Specific Projects (Nos. 2012YQ1601850 and 2013BAH42F03), Program for New Century Excellent Talents in University (No. NCET-12-0426), the Basic Research Program of Hubei Province (No. 2013CFA024), and Innovative Project of Wuhan University (2042014kf0212).

References

1. S. Hese et al., "Global biomass mapping for an improved understanding of the CO_2 balance—the Earth observation mission carbon-3D," *Remote Sens. Environ.* **94**(1), 94–104 (2005).
2. G. M. Foody, "Remote sensing of tropical forest environments: towards the monitoring of environmental resources for sustainable development," *Int. J. Remote Sens.* **24**(20), 4035–4046 (2003).
3. C. Yang, H. Huang, and S. Wang, "Estimation of tropical forest biomass using Landsat TM imagery and permanent plot data in Xishuangbanna, China," *Int. J. Remote Sens.* **32**(20), 5741–5756 (2011).
4. O. Cartus, M. Santoro, and J. Kellndorfer, "Mapping forest aboveground biomass in the Northeastern United States with ALOS PALSAR dual-polarization L-band," *Remote Sens. Environ.* **124**, 466–478 (2012).
5. L. Ji et al., "Estimating aboveground biomass in interior Alaska with Landsat data and field measurements," *Int. J. Appl. Earth Obs.* **18**, 451–461 (2012).
6. P. Propastin, "Large-scale mapping of aboveground biomass of tropical rainforest in Sulawesi, Indonesia, using Landsat ETM+ and MODIS data," *GISci. Remote Sens.* **50**(6), 633–651 (2013).
7. J.-J. Zhou et al., "Quantification of aboveground forest biomass using Quickbird imagery, topographic variables, and field data," *J. Appl. Remote Sens.* **7**(1), 073484 (2013).
8. A. Peregon and Y. Yamagata, "The use of ALOS/PALSAR backscatter to estimate aboveground forest biomass: a case study in Western Siberia," *Remote Sens. Environ.* **137**, 139–146 (2013).
9. Y. Gao et al., "Estimation of the north–south transect of Eastern China forest biomass using remote sensing and forest inventory data," *Int. J. Remote Sens.* **34**(15), 5598–5610 (2013).
10. D. Lu et al., "Relationships between forest stand parameters and Landsat TM spectral responses in the Brazilian Amazon Basin," *Forest Ecol. Manage.* **198**(1), 149–167 (2004).
11. R. J. Kauth and G. S. Thomas, "The tasselled cap—a graphic description of the spectral–temporal development of agricultural crops as seen by LANDSAT," *LARS Symposia*, Paper **159**, 41–51 (1976).

12. O. Mutanga and A. K. Skidmore, "Narrow band vegetation indices overcome the saturation problem in biomass estimation," *Int. J. Remote Sens.* **25**(19), 3999–4014 (2004).
13. S. A. Kazar and T. A. Warner, "Assessment of carbon storage and biomass on minelands reclaimed to grassland environments using Landsat spectral indices," *J. Appl. Remote Sens.* **7**(1), 073583 (2013).
14. L. Kurvonen, J. Pulliainen, and M. Hallikainen, "Retrieval of biomass in boreal forests from multitemporal ERS-1 and JERS-1 SAR images," *IEEE Trans. Geosci. Remote* **37**(1), 198–205 (1999).
15. G. Sun, K. J. Ranson, and V. I. Kharuk, "Radiometric slope correction for forest biomass estimation from SAR data in the Western Sayani Mountains, Siberia," *Remote Sens. Environ.* **79**(2), 279–287 (2002).
16. G. Sandberg et al., "L-and P-band backscatter intensity for biomass retrieval in hemiboreal forest," *Remote Sens. Environ.* **115**(11), 2874–2886 (2011).
17. S. Saatchi et al., "Impact of spatial variability of tropical forest structure on radar estimation of aboveground biomass," *Remote Sens. Environ.* **115**(11), 2836–2849 (2011).
18. P. A. Harrell et al., "Evaluation of approaches to estimating aboveground biomass in southern pine forests using SIR-C data," *Remote Sens. Environ.* **59**(2), 223–233 (1997).
19. S. Englhart, V. Keuck, and F. Siegert, "Aboveground biomass retrieval in tropical forests—the potential of combined X-and L-band SAR data use," *Remote Sens. Environ.* **115**(5), 1260–1271 (2011).
20. F. T. Ulaby et al., "Relating the microwave backscattering coefficient to leaf area index," *Remote Sens. Environ.* **14**, 113–133 (1984).
21. Y. Inoue et al., "Season-long daily measurements of multifrequency (Ka, Ku, X, C, and L) and full-polarization backscatter signatures over paddy rice field and their relationship with biological variables," *Remote Sens. Environ.* **81**, 194–204 (2002).
22. E. F. Vermote et al., "Second simulation of the satellite signal in the solar spectrum, 6S: an overview," *IEEE Trans. Geosci. Remote* **35**(3), 675–686 (1997).
23. "ESA Sentinel Toolboxes," http://nest.array.ca/web/nest (2000).
24. C. G. Chen and X. F. Guo, "Study of biomass mathematical model of broad-leaved Korean pine forest [in Chinese]," *Liaoning For. Sci. Technol.* **3**(1), 27–37 (1986).
25. J. Stéphane et al., "PROSPECT+ SAIL models: a review of use for vegetation characterization," *Remote Sens. Environ.* **113**(1), S56–S66 (2009).
26. S. Jacquemoud and F. Baret, "PROSPECT: a model of leaf optical properties spectra," *Remote Sens. Environ.* **34**(2), 75–91 (1990).
27. W. A. Allen et al., "Interaction of isotropic light with a compact plant leaf," *J. Opt. Soc. Am. A* **59**(10), 1376–1379 (1969).
28. F. Jean et al., "PROSPECT-4 and 5: advances in the leaf optical properties model separating photosynthetic pigments," *Remote Sens. Environ.* **112**(6), 3030–3043 (2008).
29. H. J. Du et al., "Retrieving crop leaf area index by combining optical and microwave vegetation indices: a feasibility analysis," *J. Appl. Remote Sens.* **17**(6), 1587–1611 (2013).
30. W. Verhoef, "Light scattering by leaf layers with application to canopy reflectance modeling: the SAIL model," *Remote Sens. Environ.* **16**(2), 125–141 (1984).
31. F. T. Ulaby et al., "Michigan microwave canopy scattering model," *Int. J. Remote Sens.* **11**(7), 1223–1253 (1990).
32. N. S. Goel and D. E. Strebel, "Simple beta distribution representation of leaf orientation in vegetation canopies," *Agron. J.* **76**(5), 800–802 (1984).
33. J. G. P. W. Clevers, "Application of a weighted infrared-red vegetation index for estimating leaf area index by correcting for soil moisture," *Remote Sens. Environ.* **29**(1), 25–37 (1989).

Linjing Zhang received her BS degree from Shandong University of Science and Technology, Shandong, China, in 2011. Currently, she is working toward her PhD degree at State Key Laboratory of Information Engineering in Surveying, Mapping and Remote Sensing, Wuhan University, China. Her research interests include forest parameters estimation and ecological environment remote sensing.

Zhenfeng Shao received his PhD degree from Wuhan University, China, in 2004. He is now a professor at State Key Laboratory of Information Engineering in Surveying, Mapping and Remote Sensing, Wuhan University, China. His research interests include remote sensing and environment monitoring.

Chunyuan Diao received her BS degree from Beijing Normal University, Beijing, China, in 2010. Currently, she is a doctoral candidate in the Department of Geography at the State University of New York at Buffalo, Buffalo, New York. Her research interests include modeling the spatial distribution of invasive species with spectral unmixing methods, and characterizing its suitable habitats with remote sensing-driven environmental models.